Ultrafast photoinduced melting of orbital order in LaVO3

doi: 10.1103/PhysRevB.68.035106

Ultrafast photoinduced melting of orbital order in $LaVO_3$

S. Tomimoto,[1] S. Miyasaka,[2] T. Ogasawara,[1] H. Okamoto,[1,3] and Y. Tokura[1,2,4]
[1]*Correlated Electron Research Center (CERC), National Institute of Advanced Industrial Science and Technology (AIST), Tsukuba 305-8562, Japan*
[2]*Department of Applied Physics, University of Tokyo, Tokyo 113-8656, Japan*
[3]*Department of Advanced Materials Science, University of Tokyo, Kashiwa 277-8561, Japan*
[4]*Spin Superstructure Project (SSS), ERATO, Japan Science and Technology Corporation (JST), Tsukuba 305-0046, Japan*
(Received 23 April 2003; published 11 July 2003)

The photoinduced effect on the orbital-ordered phase in perovskite-type $LaVO_3$ has been investigated by femtosecond time-resolved reflection spectroscopy. Large reflectivity change has been observed immediately after photoirradiation. The spectral shape and polarization dependence of the reflectivity change indicate the melting of the orbital order induced by photoexcitation. The photocarriers annihilate in about 200 fs, and the orbital order partially recovers owing to thermalization with the lattice in 2–4 ps.

DOI: 10.1103/PhysRevB.68.035106 PACS number(s): 78.47.+p, 71.27.+a

Recently, the photoinduced effect on electronic phases of correlated electron systems has aroused much interest. In several perovskite oxides, attempts to change the electronic phase by light irradiation have been made to unravel large changes of optical, magnetic, and transport properties. For example, an ultrafast insulator-metal transition by the photoinduced collapse of charge order was reported for $Pr_{0.7}Ca_{0.3}MnO_3$ (Ref. 1). In $La_{0.5}Sr_{1.5}MnO_4$ (Ref. 2) and $Nd_{0.5}Ca_{0.5}MnO_3$ (Ref. 3), the destruction of charge and orbital order by light was found to induce an immediate decrease of optical anisotropy. Furthermore, some examples of photoinduced modification of magnetic phases have recently been reported.[4,5] Ultrafast control of the electronic phase has proved those systems to be promising for high-speed device applications.

$LaVO_3$ is one of the Mott insulators which show characteristic order of d electron spin and orbital. In $LaVO_3$, the vanadium atom has the electron configuration of $3d^2$. It is known to show orbital ordering below magnetic (143 K, paramagnetic/C-type antiferromagnetic[6,7]) and structural (141 K, orthorhombic/monoclinic[8]) phase transition temperatures.[9,10] In the ordered phase, two t_{2g} electrons on the V atom occupy $d_{xy}d_{yz}$ and $d_{xy}d_{zx}$ orbitals alternately along all three directions of the lattice (G-type ordering) as represented in Fig. 1(a). The Mott-Hubbard gap transitions in perovskite vanadates are strongly dependent on ordering patterns of orbital and spin. In $LaVO_3$, they show a strong temperature dependence, reflecting the evolution of the order. In Fig. 1(c), the optical conductivity spectra of $LaVO_3$ at 10 and 293 K are shown for two light polarizations ($\mathbf{E}\|c$ and $\mathbf{E}\perp c$). The intense peak around 1.8 eV for $\mathbf{E}\|c$ at 10 K is due to the d_{yz}-d_{yz} or d_{zx}-d_{zx} transition between the neighboring V sites along the c axis which have ferromagnetic spin coupling [Figs. 1(a) and 1(b), $V_1 \rightarrow V_2$]. The intensity of this peak decreases with ascending temperature from 100 to 140 K because of orbital disordering along the c axis.[9] On the other hand, the spectrum for $\mathbf{E}\perp c$ scarcely depends on temperature. This has been accounted for in terms of the strong one-dimensional nature of the orbital exchange interaction along the c axis which arises from the antiferromagnetic spin coupling in the ab plane and the constant single occupation of the d_{xy} orbital.[11] In Fig. 2(a), the corresponding polarized reflectivity spectra are shown. As a result, the reflectivity for $\mathbf{E}\|c$ is very sensitive to the evolution of the orbital order, while that for $\mathbf{E}\perp c$ is insensitive to it. Taking advantage of this fact, we can expect to distinguish the change in the orbital order from the other photoinduced phenomena in $LaVO_3$.

We present here the result of the femtosecond time-resolved reflection spectroscopy of the perovskite vanadate $LaVO_3$. We discuss the dynamics of the photoinduced effect on the orbital-ordered phase, which includes the instantaneous melting of the orbital order, the decay of photocarriers, and the recovery of the order due to thermalization with lattice. We use the characteristic spectral shapes of the reflectivity change as a clue to distinguishing these processes and consistently explain the relaxation dynamics and its excitation density dependence.

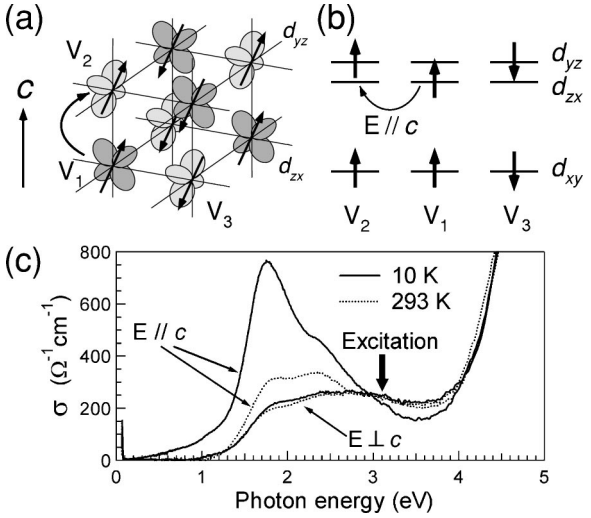

FIG. 1. (a) Schematic representation of spin and orbital ordering patterns in $LaVO_3$. (b) Electron configuration in t_{2g} orbitals at the three V sites indicated in (a). (c) Polarized optical conductivity spectra of $LaVO_3$ for $\mathbf{E}\|c$ and $\mathbf{E}\perp c$ at 10 K (solid curves) and 293 K (dotted curves). The excitation photon energy (3.1 eV) is indicated by an arrow.

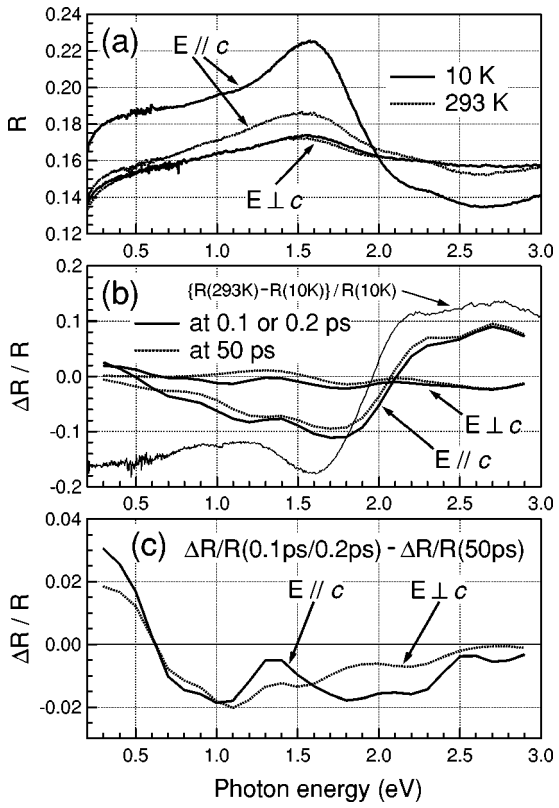

FIG. 2. (a) Polarized reflectivity spectra for $\mathbf{E}\|c$ and $\mathbf{E}\perp c$ at 10 K (solid curves) and 293 K (dotted curves). (b) Spectra of transient differential reflectivity ($\Delta R/R$) at 0.1 ps ($\mathbf{E}\perp c$) or 0.2 ps ($\mathbf{E}\|c$, thick solid curves) and at 50 ps (both polarizations, dotted curves) obtained at 7 K. A thin solid curve shows the differential reflectivity spectrum between 10 and 293 K, $\{R(293K)-R(10K)\}/R(10K)$. (c) Difference of $\Delta R/R$ between at 0.1 ps ($\mathbf{E}\perp c$) or 0.2 ps ($\mathbf{E}\|c$) and at 50 ps (7 K).

The time evolution of the polarized reflectivity change of $LaVO_3$ has been investigated by femtosecond pump-probe measurements. The light source is a Ti:sapphire regenerative amplifier system (central photon energy 1.55 eV, pulse width 100 fs, repetition rate 1 kHz). The output of this laser is divided into two beams. One is frequency doubled in a BBO crystal and used for the excitation of the sample. Another beam is used as the probe, and the photon energy is varied over a wide range (from 0.3 to 2.9 eV) by an optical parametric amplifier. The intensity of the probe pulse reflected from the sample surface is monitored as a function of the delay time relative to the pump pulse. The overall time resolution of the measurement is about 200 fs. The sample is a single crystal of $LaVO_3$ which was grown by the floating zone method as reported previously.[9] The crystal with the (100) or (010) surface was polished to optical flatness and annealed to remove mechanical stress.

In Fig. 2(b), the spectra of the transient differential reflectivity ($\Delta R/R$) immediately after photoexcitation (at delay time $t_d=0.1$ ps for $\mathbf{E}\perp c$ and 0.2 ps for $\mathbf{E}\|c$) and those at $t_d=50$ ps are shown by thick solid and dotted curves, respectively. They were obtained in the orbital-ordered phase at 7 K. The excitation photon energy is 3.1 eV, which corresponds to the high-energy side of the Mott-Hubbard gap transition band as indicated in Fig. 1(c). The electric field of the excitation light $\mathbf{E}_{ex}$ is parallel to the c axis, and the excitation density is 1.7 mJ/cm^2. As we have expected, a large and anisotropic reflectivity change is observed. For $\mathbf{E}\|c$, $\Delta R/R$ rises instantaneously up to as much as 10%. In the same figure, the spectrum of reflectivity difference between 10 and 293 K (orbital-ordered and -disordered phases, respectively) for $\mathbf{E}\|c$ is shown by a thin solid curve. The $\Delta R/R$ spectrum at 0.2 ps for $\mathbf{E}\|c$ is very similar to the differential spectrum. For $\mathbf{E}\perp c$, on the other hand, the $\Delta R/R$ is very small throughout the observed energy range. The similarity to the differential spectrum for $\mathbf{E}\|c$ as well as the large anisotropy indicates that the rise of $\Delta R/R$ for $\mathbf{E}\|c$ arises chiefly from the destruction of the orbital order upon photoexcitation. The $|\Delta R/R|$ for $\mathbf{E}\|c$ gradually decreases below 1.3 eV and deviates from the differential spectrum. This can be attributed to the mismatch of the penetration depth between the pump and probe lights. The depth of the probe light, l_{pr}, becomes longer than that of the pump light ($l_{ex}=280$ nm) below 1.3 eV because the optical conductivity for $\mathbf{E}\|c$ [Fig. 1(c)] decreases with a decrease of energy in that energy region ($l_{pr}=400$ nm at 1.3 eV and $l_{pr}=2700$ nm at 0.5 eV).

In addition to the signals related to the orbital order, we have observed another component which decays very fast within 1 ps. To clarify the origin, the spectra of this component have been extracted by subtracting $\Delta R/R$ at 50 ps from that at 0.1 ps ($\mathbf{E}\perp c$) or 0.2 ps ($\mathbf{E}\|c$). The result is shown in Fig. 2(c). This component is negative from 0.6 to 2.9 eV for both probe polarizations. As the excitation energy is 3.1 eV, the negative $\Delta R/R$ over this wide energy range seems to be due to the bleaching of the optical absorption from the electronic ground state. Below 0.6 eV, positive $\Delta R/R$ is observed, indicating that the spectral weight of the gap transition is transferred to the inner-gap region. These two features of the spectra suggest that the fast component within 1 ps originates from the generation and decay of photocarriers.

Figure 3 shows the time dependence of $\Delta R/R$ at 1.0 eV for two different excitation densities (0.42, 2.6 mJ/cm^2). As it does not show an obvious dependence on the excitation polarization, we present here the data for $\mathbf{E}_{ex}\|c$. The temporal dynamics depends strongly on the excitation density. Figure 4(a) shows the dependence of $|\Delta R/R|$ for $\mathbf{E}\|c$ on the excitation density monitored at three typical delay times 0.15, 50, and 6000 ps. There are three regions of the excitation density which show qualitatively different dependence on the density: (1) linear response region ($\leqslant 0.6$ mJ/cm^2), (2) nonlinear response region (0.6–3 mJ/cm^2), and (3) saturation region ($\geqslant 3$ mJ/cm^2).

In region (1), $\Delta R/R$ increases linearly with excitation density at all the delay times. Thus, the temporal dynamics of $\Delta R/R$ does not depend on the density in this region. As indicated by an arrow in Fig. 4(a), the excitation density of 0.42 mJ/cm^2 which was used to obtain the data set in Figs. 3(a) and 3(b) is close to the upper limit of this region. The time dependence at this density [Figs. 3(a) and 3(b)] can be fitted by the double-exponential decay plus a constant term, $I(t)=I_1e^{-t/\tau_1}+I_2e^{-t/\tau_2}+I_3$. The fitting is performed with

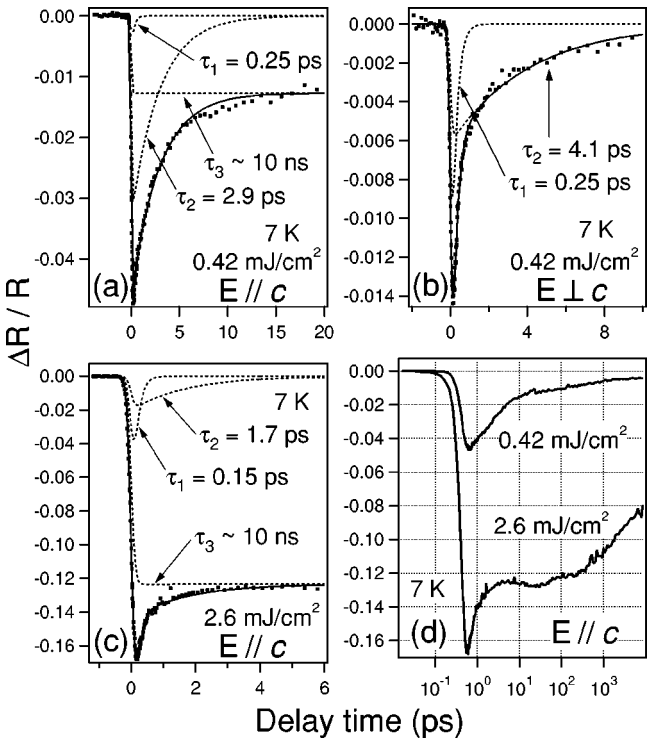

FIG. 3. Time dependence of $\Delta R/R$ at 1.0 eV (7 K): (a) probe polarization $\mathbf{E}\|c$, excitation density 0.42 mJ/cm^2, (b) $\mathbf{E}\perp c$, 0.42 mJ/cm^2, and (c) $\mathbf{E}\|c$, 2.6 mJ/cm^2. Dots are experimental data. Solid curves show the fitting with a few exponential decay components. The components with respective lifetimes are shown by dashed curves. (d) Experimental data for $\mathbf{E}\|c$ at two indicated excitation densities. To show them on a logarithmic time scale, the time origin is shifted by 0.4 ps from the other panels.

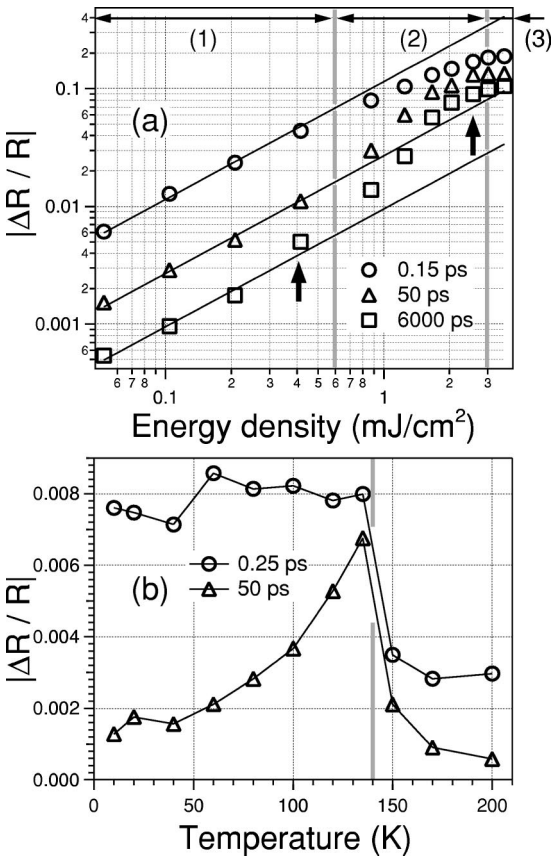

FIG. 4. (a) Dependence of $|\Delta R/R|$ for $\mathbf{E}\|c$ at 1.0 eV on excitation energy density, monitored at 0.15, 50, and 6000 ps at 7 K. The excitation density can be sorted into three regions: (1) linear response region, (2) nonlinear response region, and (3) saturation region. The lines show linear relationship between $|\Delta R/R|$ and excitation density. (b) Temperature dependence of $|\Delta R/R|$ for $\mathbf{E}\|c$ at 1.0 eV monitored at 0.25 and 50 ps. The excitation density is 0.4 mJ/cm^2.

the convolution of this equation with the response function of the measurement system. In the figures, the fitting curves and decay components are shown with solid and dashed curves, respectively. As mentioned above, the first term ($\tau_1 = 0.25$ ps) corresponds to the decay of the bleaching of the electronic ground state. This component appears more clearly for $\mathbf{E}\perp c$. It decays rapidly with a decrease of photocarriers. The second term expresses a decay component with a little longer lifetime. It appears for both probe polarizations with almost the same lifetimes (2.9 ps for $\mathbf{E}\|c$, and 4.1 ps for $\mathbf{E}\perp c$). This decay component can be ascribed to the thermalization process of the system because, after it decays, $\Delta R/R$ hardly changes for about 1 ns. As this component is polarized along the c axis and is sensitive to the change of the orbital order, its temporal decay stands for the partial recovery of the orbital order through the thermalization. This process is expected to occur via the coupling of agitated orbital order with lattice dynamics due to the Jahn-Teller interaction. The last constant term appears only for $\mathbf{E}\|c$. This term represents the component which shows nonexponential slow decay and survives longer than 10 ns [Fig. 3(d), 0.42 mJ/cm^2]. As the orbital-lattice system is thermalized in a few picoseconds, we consider this component as due to the heating of the macroscopic volume of the sample near the surface. As can be seen in Figs. 3(a) and 3(b), the temporal dynamics can be approximated by assuming that all the three components rise instantaneously. Both the second and third components are due to the photoinduced melting of the orbital order. Thus, the instantaneous rise of their sum indicates that the destruction of the order is adiabatically induced within the time resolution (about 200 fs). By comparing the $\Delta R/R$ with the differential reflectivity between 10 and 293 K [Fig. 2(b)], we estimate that one excitation photon induces the disordering of t_{2g} orbitals over about 60 V sites instantaneously in region (1).

In Fig. 4(b), the temperature dependence of $|\Delta R/R|$ for $\mathbf{E}\|c$ monitored at 0.25 and 50 ps is shown. The excitation density is 0.4 mJ/cm^2 in region (1). The $|\Delta R/R|$ abruptly decreases around 140 K above which the d_{yz}/d_{zx} orbital shows no long-range order. This assures again that the observed signal is mainly due to the melting of the orbital order. The signal after the thermalization (at 50 ps) increases with raising the temperature up to 140 K. This is because the energy flow to the lattice and the recovery of the orbital order during the thermalization tend to be suppressed with increasing lattice temperature.

In the excitation density region (2) in Fig. 4(a), $\Delta R/R$ at 0.15 ps begins to saturate. But the $\Delta R/R$ at 50 ps and at 6000

ps shows a nonlinear increase with the ascent of excitation density. In Fig. 3(c), the time dependence of $\Delta R/R$ for $\mathbf{E}\|c$ is shown for the excitation density of 2.6 mJ/cm^2 which is close to the upper limit of region (2) [indicated by an arrow in Fig. 4(a)]. The temporal dependence can be well expressed as a double-exponential decay with lifetimes of 0.15 ps ($=\tau_1$) and 1.7 ps ($=\tau_2$) and a constant term. All three components rise within the time resolution (about 200 fs). The intensity of the constant term relative to the second decay component is much larger than that in the linear region (1). Most of the $\Delta R/R$ signal due to the disordering of orbitals (the sum of the second and third terms) remains longer than 10 ps. The result shows that the orbital order hardly recovers in such a short time period through thermalization with the lattice at this high excitation density. A detailed analysis of the optical conductivity spectra has revealed that the orbital order grows up steeply from 140 K to 120 K (Ref. 9). Therefore, whether the temperature of the thermalized state is lower than 120 K or not should determine whether the orbital order can recover. From the specific heat of $LaVO_3$ (Ref. 12), we estimate that an energy of about 3500 J/mol is necessary to heat from 7 K to 120 K. Taking the penetration depth of the excitation light ($l_{ex}=280$ nm) and the reflection loss ($R=0.14$) into consideration, this corresponds to an excitation density of 0.67 mJ/cm^2. This agrees well with the lower boundary of region (2). Thus, in this region, the temperature will become higher than the critical one (120 K). Then, as shown in Fig. 4(a), the $|\Delta R/R|$ after thermalization (for example, at 50 and 6000 ps) exhibits a nonlinear increase with the ascent of excitation density. This component has a lifetime of about 10 ns [Fig. 3(d), 2.6 mJ/cm^2] and decays with progress of the thermal diffusion. The lifetime is reasonable if we assume a temperature gradient of 120 K/280 nm and heat conductivity of ~ 1 W/mK (Ref. 13).

As can be seen in Fig. 4(a), the $\Delta R/R$ signal saturates in region (3) at all delay times. In this region, the reflectivity change for $\mathbf{E}\|c$ reaches as much as 15% even in the thermalized state [Fig. 4(a), at 50 ps]. As the difference of reflectivity between 10 and 293 K at 1.0 eV is about 15% [Fig. 2(b)], this shows that most of the orbital correlation is lost upon the photoexcitation in this density region.

The dynamics after photoexcitation can be characterized by the following four processes: (1) photocarrier generation and melting of orbital order ($\ll 200$ fs), (2) annihilation of photocarriers (about 200 fs), (3) partial recovery of the agitated orbital order due to thermalization with the lattice (2–4 ps), and (4) cooling of the system due to thermal diffusion (about 10 ns). The most important feature in the dynamics is the ultrafast melting of the orbital order, which is induced by the injection of minor photocarriers and spreads over 60 V sites per photon.

In summary, the photoinduced effect on the orbital-ordered phase of $LaVO_3$ has been studied by femtosecond reflection spectroscopy. The spectral shape and polarization dependence of the transient reflectivity change demonstrate the melting of the orbital order induced immediately after photoexcitation. The observed ultrafast and large optical response clearly shows the high potential of orbital-ordered Mott insulators for optical switching units.

We thank S. Iwai for helpful discussions. This work has been partially supported by the NEDO of Japan.

[1] M. Fiebig, K. Miyano, Y. Tomioka, and Y. Tokura, Appl. Phys. B: Lasers Opt. **71**, 211 (2000).
[2] T. Ogasawara, T. Kimura, T. Ishikawa, M. Kuwata-Gonokami, and Y. Tokura, Phys. Rev. B **63**, 113105 (2001).
[3] T. Ogasawara, K. Tobe, T. Kimura, H. Okamoto, and Y. Tokura, J. Phys. Soc. Jpn. **71**, 2380 (2002).
[4] K. Matsuda, A. Machida, Y. Moritomo, and A. Nakamura, Phys. Rev. B **58**, R4203 (1998).
[5] R.D. Averitt, A.I. Lobad, C. Kwon, S.A. Trugman, V.K. Thorsmølle, and A.J. Taylor, Phys. Rev. Lett. **87**, 017401 (2001).
[6] V.G. Zubkov, G.V. Bazuev, V.A. Perelyaev, and G.P. Shveikin, Sov. Phys. Solid State **15**, 1079 (1973).
[7] G. Khaliullin, P. Horsch, and A.M. Oleś, Phys. Rev. Lett. **86**, 3879 (2001).
[8] P. Bordet, C. Chaillout, M. Marezio, Q. Huang, A. Santoro, S-W. Cheong, H. Takagi, C.S. Oglesby, and B. Batlogg, J. Solid State Chem. **106**, 253 (1993).
[9] S. Miyasaka, Y. Okimoto, and Y. Tokura, J. Phys. Soc. Jpn. **71**, 2086 (2002).
[10] H. Sawada, N. Hamada, K. Terakura, and T. Asada, Phys. Rev. B **53**, 12 742 (1996).
[11] Y. Motome, H. Seo, Z. Fang, and N. Nagaosa, Phys. Rev. Lett. **90**, 146602 (2003).
[12] A.S. Borukhovich, G.V. Bazuev, and G.P. Shveikin, Sov. Phys. Solid State **15**, 1467 (1974).
[13] J.L. Cohn, J.J. Neumeier, C.P. Popoviciu, K.J. McClellan, and Th. Leventouri, Phys. Rev. B **56**, R8495 (1997).